Conference Paper, Published Version

Ligier, Pierre-Louis

Implementation of non-Newtonian rheological models in TELEMAC-2D

Implementation of non-Newtonian rheological models in TELEMAC-2D

Pierre-Louis Ligier
Power Generation and Dams Department
Sweco Energy AB
Stockholm, Sweden
pierre-louis.ligier@sweco.se

***Abstract*—Sediment transport modelling in hydrodynamic models is based on the assumption that the sediment concentration remains sufficiently low so that the flow behaviour remains Newtonian, i.e. that the fluid is assumed to keep the same properties as water. This assumption is valid for sediment volumetric concentrations up to approximatively 20-30%. For larger concentrations, the flow behaviour can no longer be assumed to remain Newtonian and non-Newtonian rheological flow models are required to provide a more accurate modelling of the fluid behaviour. This article presents the implementation of such models in the two-dimensional hydrodynamic model TELEMAC-2D. The considered field of application is primarily the modelling of mudflows such as tailings dam failures with release of liquefied tailings in which the sediment volumetric concentrations are commonly larger than 40%. Two models have been implemented: the classic Bingham viscoplastic model and the more general Herschel-Bulkley model. Both models exhibit a plastic behaviour through the yield stress parameter that acts as a threshold for the onset of fluid motion. Once the shear stress exceeds the fluid's yield stress, the flow behaviour becomes viscous and governed by a simple constant viscosity assumption for the Bingham model whereas in the Herschel-Bulkley model, viscosity is described with a power-law. The resulting shear stress is treated as a friction slope source term applied to the two-dimensional momentum equations. The implementation offers the possibility to model the non-Newtonian rheological properties either constant in space and time (i.e. non-Newtonian fluid with constant rheological properties) or variable in space and time using a pseudo-biphasic, variable-density formulation in which the rheological properties (density, yield stress and viscosity) are computed from the local sediment volumetric concentration. Validation and application examples are presented in order to highlight the capabilities and limitations of the implemented models. The article also contains an application example of the Brumadinho tailings dam failure that occurred in Brazil in January 2019 with comparison against field observations as well as results from simulations performed with other software.**

I. INTRODUCTION

Modelling of classic sediment transport in hydrodynamic models is based on the assumption that the sediment concentration remains sufficiently low so that the flow behaviour remains Newtonian, i.e. that the fluid is assumed to keep the same properties as water. This assumption is valid for sediment volumetric concentrations up to approximatively 20-30% [1] [2]. For larger concentrations, the flow behaviour can no longer be assumed to remain Newtonian and non-Newtonian rheological flow models are required to provide a more accurate modelling of the fluid behaviour. The behaviour of a Newtonian fluid is defined by a linear relationship between the shear (viscous) stress τ_0 [Pa] and the shear rate $\dot{\gamma}$ [s^{-1}]:

$$\tau_0 = \mu\dot{\gamma} \quad (1)$$

with μ the fluid's dynamic viscosity [Pa·s]. For non-Newtonian fluids, the relationship between the shear stress and the shear rate is no longer linear and can exhibit complex behaviours (plastic, dilatant, contractant…). The rheological properties of non-Newtonian fluids can generally be described by their density, their viscosity which can vary depending on the actual strain and shear stress rates and, for some non-Newtonian models, by a yield stress. For such models, the fluid starts to flow when the actual shear stress exceeds the fluid's yield stress, otherwise the fluid stops moving and behaves as a solid. The yield stress is often referred to as a threshold value for the onset of motion. Examples of several types of Newtonian and non-Newtonian fluid behaviours are presented in Fig. 1 in a so-called shear rate-shear stress diagram.

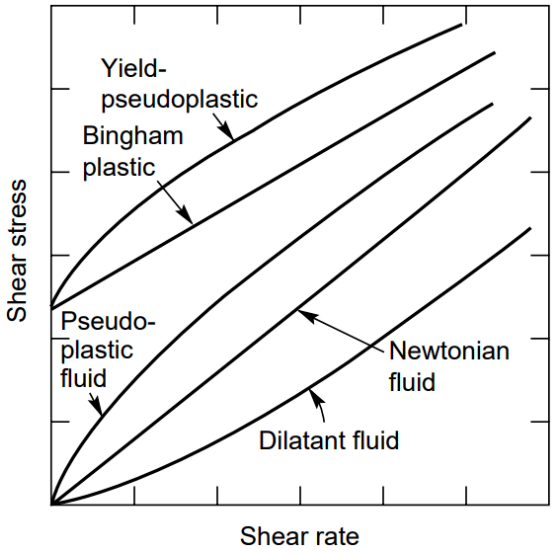

Figure 1: Examples of Newtonian and non-Newtonian fluids behaviour in a shear rate-shear stress diagram (taken from [6]).

One of the most classical non-Newtonian fluid models is the so-called Bingham or "Bingham plastic" fluid model. This model is well suited for homogeneous suspensions of fine particles, particularly mudflows, under low rates of deformation [2] and is also commonly accepted for modelling flowing tailings [3] [4]. A more generic non-Newtonian model is the Herschel-Bulkley model (yield-pseudoplastic) which combines the effects of the Bingham model with a yield stress and power-law behaviour. This model is suitable for modelling shear-thinning behaviour that some tailings slurries exhibit (loss of shear strength with increasing shear rates) [5]. Both models have been implemented in TELEMAC-2D. This article presents the theoretical background behind these two models as well as their implementation into the software. Finally, validation and application examples are provided.

II. THE BINGHAM MODEL

A. Formulation

The equation of the Bingham model reads:

$$\begin{cases} \dot{\gamma} = 0 & if \ \ \tau_0 \leq \tau_y \\ \tau_0 = \tau_y + \mu\dot{\gamma} & if \ \ \tau_0 > \tau_y \end{cases} \quad (2)$$

with τ_y the fluid's yield stress [Pa]. Within the 1D and 2D modelling framework, it is common to use the quadratic rheological model proposed by O'Brien and Julien (1985) which defines the total shear stress of the flow τ as the sum of the yield and viscous stresses induced by the non-Newtonian behaviour (i.e. τ_0) and of the turbulent stresses induced by bottom friction [2] [7] [8]. One assumption of the quadratic rheological model is that the shear rate $\dot{\gamma}$ is defined as du/dz, that is the velocity gradient in the vertical direction, neglecting gradients in the horizontal plane. Assuming that the flow is laminar, the shear rate can then be approximated as [8]:

$$\dot{\gamma} = du/dz = 3U/h \quad (3)$$

with u the components of the three-dimensional velocity vector [m/s], U the depth-averaged flow velocity [m/s] and h the flow depth [m]. Another approach consists in expressing the last term of (3) as follows [7]:

$$\dot{\gamma} = \frac{KU}{8h} \quad (4)$$

with K a resistance parameter for laminar flow [-]. Its value lies in the range 24-108 for smooth surfaces (concrete, asphalt) but can increase significantly with irregular geometry and roughness (highest values of approximatively 50 000) [7]. It can be observed that with the lowest value, of 24, (4) is reduced to (3). This resistance parameter has been proposed within the framework of overland runoff by Woolhiser (1975) (see also [9]) and should therefore be used in accordance with the underlying assumptions. When modelling turbulent flows, the lowest value of 24 is therefore recommended. However, the resistance parameter can also be used as an empirical coefficient in order to adjust the theoretical "laminar" shear rate to take 2D and 3D effects into account (stronger vertical velocity gradient, horizontal subgrid-gradient, etc.).

Even though the Bingham model's mathematical expression is relatively simple, the discontinuity generated by the yield stress parameter at very low shear rates is a disadvantage and can lead to numerical instabilities. To solve this issue, several solution methods have been proposed in the literature, aiming at replacing the discontinuity by a continuous relationship between shear stress and shear rate. Three of such methods, called "Options" in this article, have been implemented, and are described in the next section.

B. Solution methods

Option 1: exponential regularization

This method is based on the exponential regularization method proposed by Papanastasiou (1987) [10] [11]. An exponential term is added to the yield stress parameter making it possible to introduce a continuous relationship for low shear rates:

$$\tau_0 = \tau_y\left(1 - e^{-m\dot{\gamma}}\right) + \mu\dot{\gamma} \quad (5)$$

with m a so-called regularization parameter [s] used to control the exponential growth of shear stress for low shear rates. The effect of the regularization parameter is illustrated in Fig. 2 in which the shear stress is normalized by the yield stress. For high values of m, the classical Bingham model is retrieved whereas as m tends towards zero, the model reduces to a linear, Newtonian fluid behaviour. The value of m has been set to 1000 s as proposed in [11]. The shear rate is computed using (4) based on a user-defined value for the resistance parameter for laminar flow K (default value is 24).

Option 2: effective viscosity

This method is based on the effective viscosity concept by rewriting the Bingham model (2) as:

$$\tau_0 = \mu_{eff}\dot{\gamma} \quad (6)$$

with μ_{eff} the effective viscosity [Pa·s], defined by the following set of equations, based on the so-called Cross formulation [8] [12]:

$$\mu_{eff} = \frac{\mu_0 + \mu K_B \dot{\gamma}}{1 + K_B \dot{\gamma}} \quad (7)$$

$$K_B = \mu_0/\tau_y \quad (8)$$

$$\mu_0 = 10^3\mu \quad (9)$$

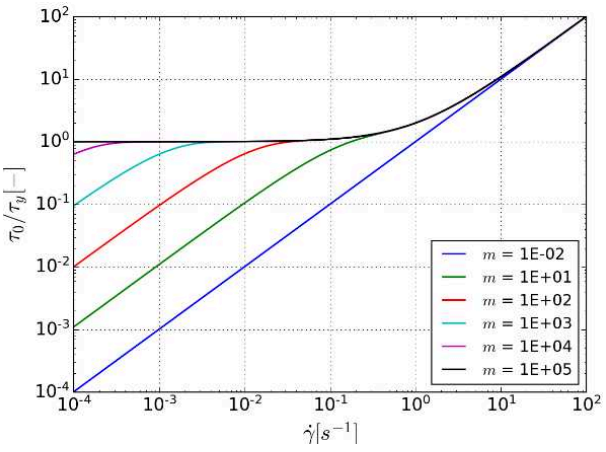

Figure 2: Bingham model, Option 1 (exponential regularization). Influence of the regularization parameter m.

The shear rate is computed using (4) based on a user-defined value for the resistance parameter for laminar flow K (default value is 24).

Option 3: Bingham cubic equation

This method is based on a cubic equation for the non-Newtonian shear stress that is obtained from the integration of the classical Bingham equation for laminar flow in a wide open channel, and then solving for the depth-averaged flow velocity as proposed by Rickenmann [13] and cited in [14] and [15]. The resulting cubic equation reads:

$$2{\tau_0}^3 - 3{\tau_0}^2\left(\tau_y + 2\mu\, U/h\right) + {\tau_y}^3 = 0 \qquad (10)$$

This equation is solved using the `CUBEEQUATION` subroutine available in the TELEMAC-2D library (`.\sources\telemac2d`), keeping the positive root closest from the theoretical value of τ_0 defined by (2).

Comparison between the three different options

The flow behaviour curves for the three options implemented described above are illustrated in Fig. 3 in which the shear stress is normalized by the yield stress. For Options 1 and 2, the resistance parameter for laminar flow K is set to its default value of 24. It can be observed that Options 1 and 2 correspond to a similar flow behaviour with only minor differences being observed at very low shear rates. The flow behaviour obtained with Option 3 is the closest to the theoretical Bingham model (2) at very low shear rates but yields an approximatively 5%-25% larger shear stress for shear rates in the range 10^{-2}-10^{1} s^{-1}, which corresponds to usual values (see also Fig. 4).

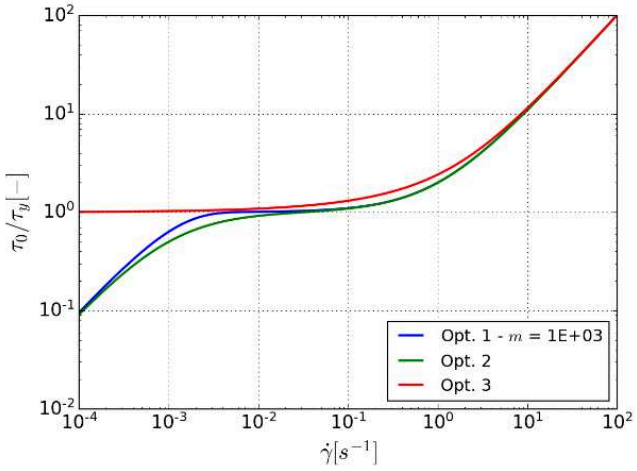

Figure 3: Bingham model, comparison between the three options implemented.

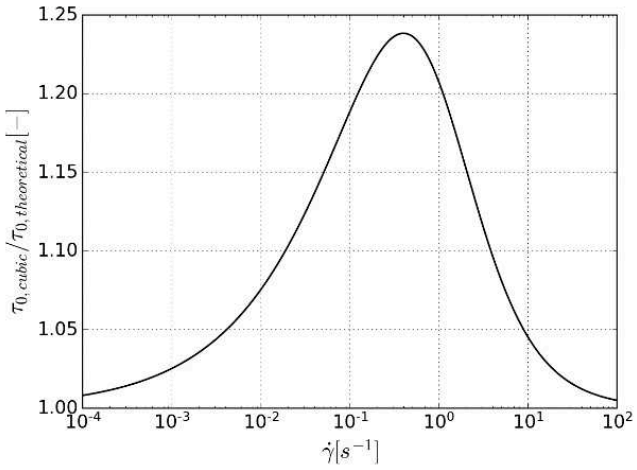

Figure 4: Bingham model, comparison between shear stress computed with cubic equation (Option 3) and theoretical values.

III. THE HERSCHEL-BULKLEY MODEL

A. Formulation

The equation of the Herschel-Bulkley model reads:

$$\begin{cases} \dot{\gamma} = 0 & if \;\; \tau_0 \leq \tau_y \\ \tau_0 = \tau_y + K_{HB}\dot{\gamma}^n & if \;\; \tau_0 > \tau_y \end{cases} \qquad (11)$$

with K_{HB} the consistency parameter [Pa·s] and n the power-law index [-]. The Bingham model can be retrieved if $K_{HB} = \mu$ and $n = 1$.

B. Solution method

The Herschel-Bulkley model has been implemented using the exponential regularization method also used for the Bingham model (Option 1), as proposed in [10]:

$$\tau_0 = \tau_y\left(1 - e^{-m\dot{\gamma}}\right) + K_{HB}\dot{\gamma}^n \qquad (12)$$

As for the Bingham model, the value of the regularization parameter m has been set to 1000 s (see section II-B). The shear rate is computed using (4) based on a user-defined value for the resistance parameter for laminar flow K (default value is 24).

IV. IMPLEMENTATION IN TELEMAC-2D

The non-Newtonian shear stress computed by the non-Newtonian models is expressed as a friction slope using the following equation:

$$S_0 = \frac{\tau_0}{\rho g h} \qquad (13)$$

with S_0 the friction slope [-] corresponding to the non-Newtonian shear stress, ρ the fluid's bulk density [kg/m^3] and g the gravity acceleration [m/s^2]. The friction slope term S_0 is then multiplied by g and inserted in the momentum equations' source terms S_x and S_y [m/s^2]. The source terms are treated semi-implicitly to ensure numerical stability even in regions with strong gradients (e.g. wave front). A drawback of this treatment is numerical diffusion which can lead to a loss of accuracy especially in regions where the non-Newtonian stresses are dominant. For a thorough overview of the two-dimensional equations solved by TELEMAC-2D, please refer to [16] and [17].

In its current status, the non-Newtonian models have only been implemented in the Finite Volume version of TELEMAC-2D. The non-Newtonian source term is treated semi-implicitly, as for bottom friction, in a new subroutine called `NONNEWT_FV` called from `SOURCE_MOMENT`.

Tests have also been performed in Finite Elements but showed poor results with instabilities in areas with strong gradients, i.e. with small mesh sizes and/or for large values for yield stress and dynamic viscosity. However, reasonable results that compared well with Finite Volume have been obtained on dam break simulations with very large mesh sizes. Further work is required before the non-Newtonian models can also be included in TELEMAC-2D's Finite Element version.

V. PSEUDO-BIPHASIC, VARIABLE DENSITY FORMULATION

In practical applications for tailings dam break studies, the assumption of non-Newtonian rheological parameters constant in time and space can be limiting especially if the flood wave flows into lakes and/or rivers. In order to take mixing effects into account, a simplified pseudo-biphasic, variable density formulation has been implemented.

The principle of this formulation is to determine the fluid density and the rheological parameters (yield stress and dynamic viscosity) from the local sediment volumetric concentration C_V [-]. The sediment volumetric concentration typically ranges between 0.0-0.2 for water floods with suspended sediment, 0.2-0.45 for mud floods, 0.45-0.55 for mudflows, flowing tailings and 0.55-0.8 for landslides [1] [2]. Furthermore, this formulation is based on the underlying assumption that the sediment is transported in suspension through advection and dispersion with a nil settling velocity and without interaction with the bed (no erosion/deposition).

The type of fluid can therefore be defined by the local sediment volumetric concentration C_V. The local fluid's bulk density is then computed as:

$$\rho = \rho_W + (\rho_S - \rho_W)C_V \quad (14)$$

with ρ_W the water density [kg/m^3] and ρ_S the sediment specific density (grains) [kg/m^3].

In this formulation, the local sediment volumetric concentration C_V is to be defined by the user via a passive tracer (with initial and boundary conditions). The mixing between the different fluid mixtures defined by different values of C_V is therefore governed by the advection and diffusion of the passive tracer. The main limitation of this method is that diffusion at the interface between two fluids, and therefore mixing, is overestimated.

Empirical relationships have been proposed to express the yield stress and the dynamic viscosity as functions of the sediment volumetric concentration C_V [2]:

$$\tau_y = a10^{bC_V} \quad (15)$$

$$\mu = c10^{dC_V} \quad (16)$$

The values of the coefficients a, b, c and d are mainly function of the nature and percentage of fine particles in the mixture. Experimental values have been proposed in the literature ([2] [7] [18]).

When the pseudo-biphasic formulation is used, (15) and (16) are applied at every wet node regardless of the local value of C_V. In practical cases, the values of the coefficients a, b, c and d are such that the resulting yield stress and dynamic viscosity computed with low C_V values can be considered representative of a Newtonian fluid (i.e. the corresponding non-Newtonian shear stress is negligible). The values of the coefficients a, b, c and d should be defined in subroutine `NONNEWT_FV`.

VI. VALIDATION EXAMPLES

A. Deposition of a thickened tailings slurry

The first case used to test the non-Newtonian models implemented is the reproduction of the deposition of a thickened tailings slurry. The case used is taken from [4] for which an analytical solution is available. The set-up consists of releasing a tailings slurry with a constant discharge of 26.46 l/min in a 150 mm wide flume with a flat and smooth bottom. The slurry discharge is applied for 12 s before the fluid deposits and reaches an equilibrium profile. In the case, the slurry is released from a 21 mm x 21 mm opening and falls vertically on the bottom of the plume. In the simulation, the discharge is instead applied through a 25 mm-wide lateral open boundary centered on the flume axis at X = 0 m. The computational mesh is 150 mm wide and 2000 mm long with a mesh size of 5 mm. The fluid properties are taken from measurements and are as follows: bulk density ρ = 1315 kg/m^3, yield stress τ_y = 18.6 Pa and dynamic viscosity μ = 0.32 Pa·s.

The simulations have been performed with the Bingham model for the three options implemented using the kinetic finite volume scheme (FINITE VOLUME SCHEME = 1) [19]. Bottom friction has been simulated with a Strickler coefficient of 70 m$^{1/3}$/s to mimic the smooth plume bottom. The standard slip condition on the lateral solid boundaries was used in order to comply with the assumptions used in the Slow Sheet Flow (SSF) model and the "Case 3" from the CFD simulations performed in [4]. It is worth noting that the SSF model is based on the assumption that the inertial effects of the flow are negligible [4]. The slow flow conditions used in the flume test are assumed to comply with this assumption.

The results are presented as flow profiles at three different times (after 12 s, 14 s and 20 s) and compared with the analytical solution of the SSF model in Fig. 5. The first observation from the results is that in the simulation, the fluid never reaches a true equilibrium profile unlike what can be observed in the experiments and assumed in the SSF model. The analysis of the simulated flow profiles shows that the shape of the slurry is well reproduced with a well-defined and steep wave front up to 14 s. After this time, the front starts to spread out in the downstream direction while the overall profile shape remains nearly constant. The cause of the lack of equilibrium state in the simulation is linked to the numerical method used to model the flow shear stress (semi-implicit treatment of the non-Newtonian source term, see section IV), in which flow velocity, although being very small, never reaches zero. A similar behaviour was observed in the CFD simulations from [4]. The comparison between the three different Bingham model options implemented shows that the Options 1 and 2 give very similar results, which is expected (see section II-B). The flow profiles after 12 s match well the

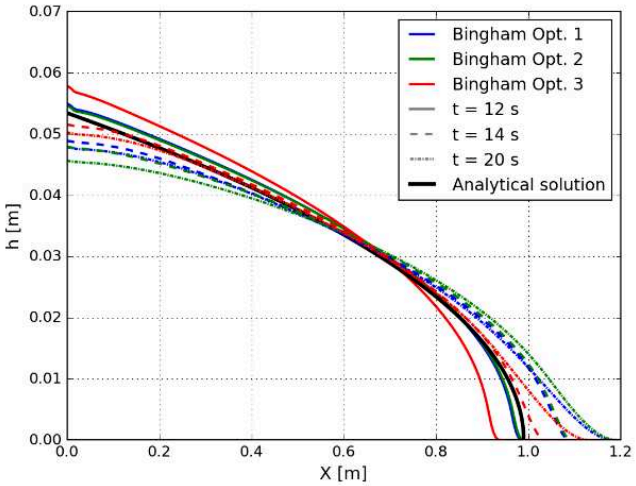

Figure 5: Deposition of thickened tailings, results of Bingham model after 12 s, 14 s and 20 s and analytical solution.

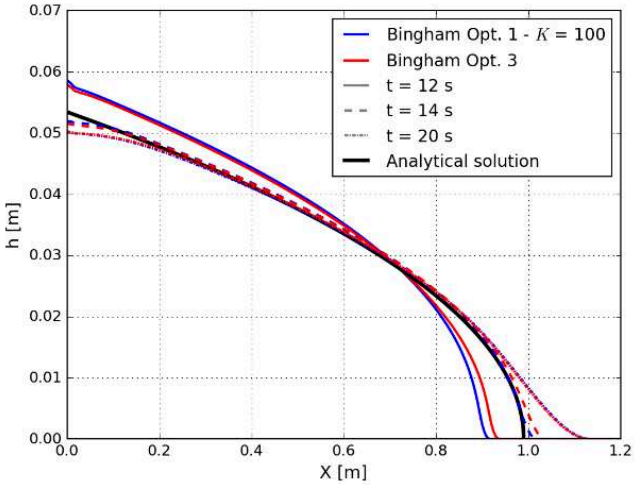

Figure 6: Deposition of thickened tailings, influence of the resistance parameter for laminar flow K.

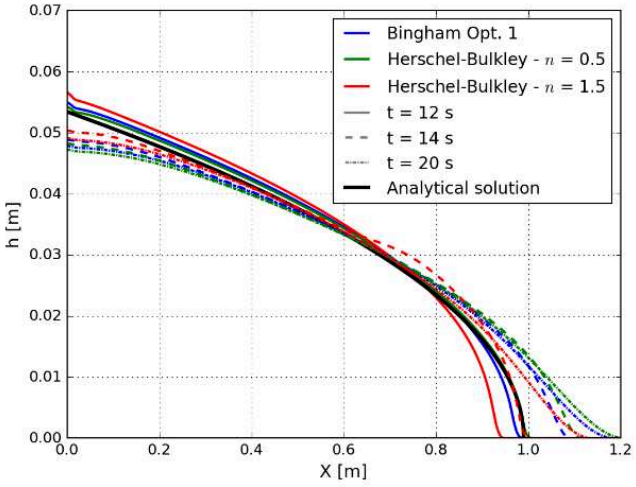

Figure 7: Deposition of thickened tailings, comparison between Bingham and Herschel-Bulkley models.

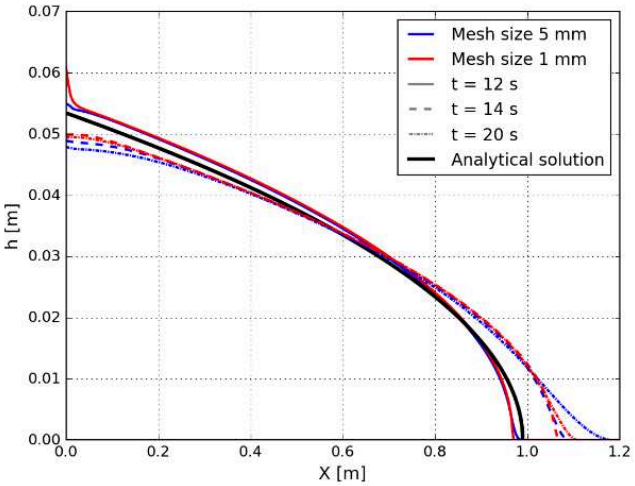

Figure 8: Deposition of thickened tailings, influence of mesh size (Bingham Option 1).

analytical solution but the profiles continue to stabilize until approximatively 14 s where they reach a pseudo-equilibrium excepted for the front that continues to spread out. The flow profiles at 14 s lie within approximatively 10% of the analytical solution (front distance overestimated, flow depth at X = 0 m underestimated). The Option 2 shows however more spreading than Option 1 at 14 s, which is also expected as this option has a smoother transition towards the yield stress at low shear rates than Option 1. The Option 3 shows the best agreement with the analytical solution, with flow profiles located less than 5% from the SSF model. The more resistive behaviour of the Option 3 compared to Options 1 and 2 was expected as the Bingham cubic equation yields shear stresses that are 5-25% larger than theoretical values at usual shear rates (see section II-B). In comparison, the CFD simulation "Case 3" from [4] shows a flow profile with a front location approximatively 5% shorter than the analytical solution.

In order to test the sensibility of the Option 1 to the resistance parameter for laminar flow K, a simulation was performed with $K = 100$ which corresponds to the upper range for smooth surfaces. The result shows that the larger viscous stresses induced by this set-up steepens up the flow profile which lies very close from the analytical solution and from the result of Option 3 once pseudo-equilibrium is reached at 14 s (Fig. 6).

This case has also been simulated with the Herschel-Bulkley model in which the consistency parameter K_{HB} was taken equal to the dynamic viscosity used in the Bingham simulations. Two simulations were performed with power-law index values of $n = 0.5$ and $n = 1.5$. The results are compared qualitatively with the Bingham Option 1 in Fig. 7 for the flow profiles at 14 s. As expected, a power-law index smaller than 1 ($n = 0.5$) shows a flatter, less resistive, profile whereas a power-law index larger than 1 ($n = 1.5$) shows a steeper, more resistive, profile.

Finally, the case has been run on a finer mesh to analyse the influence of mesh size on the results. The finer mesh has a 1 mm node spacing in the flow direction. Results for Bingham

Option 1 with mesh sizes 1 and 5 mm are presented in Fig. 8. The finer mesh gives very similar results than the original mesh for the flow profiles corresponding to 12 and 14 s, with a slight improvement of the front region which becomes steeper. However, a noticeable improvement is visible on the flow profile at 20 s where the finer mesh significantly limits the spreading of the front (10% shorter distance and front slope well preserved).

The results presented above show that the non-Newtonian models implemented in TELEMAC-2D can reproduce the behaviour of tailings slurry until a pseudo-equilibrium state is reached in a satisfactory way. Results compare well with the analytical solution and results from CFD simulations (for further details, please refer to [4]). Result analysis should take the numerical spreading occurring after pseudo-equilibrium is reached into account.

B. One-dimensional dam break

The one-dimensional dam break case presented in [20] is used to test the implemented non-Newtonian models for such applications. This dam break case has also been used as a validation case for the numerical code DFEM-1D in which several non-Newtonian models have been implemented [14]. The dam break case corresponds to the instantaneous release of a non-Newtonian fluid defined by a volume of 305 m in length (in the flow direction) and 30.5 m in height on a flat, dry and smooth bottom. The fluid properties used in [14] are a fluid density ρ = 1835 kg/m^3, a yield stress τ_y = 1500 Pa and a dynamic viscosity μ = 100 Pa·s. The theoretical solution of this case provided by Hungr [20] and based on the assumption that the flow profile after reaching equilibrium is parabolic, gives a front location of X = 1896 m counted from X = 0 m, which corresponds to a runout distance of 1591 m counted from the dam location (X = 305 m).

This case was simulated using a two-dimensional triangular mesh with an element size of 3 m in both X and Y directions. The model is 3000 m long in the X direction and 12 m wide in the Y direction. The simulations have been performed with the Bingham model for the three options implemented using the HLLC finite volume scheme (FINITE VOLUME SCHEME = 5) [21]. Bottom friction has been simulated with a Strickler coefficient of 70 m$^{1/3}$/s to mimic the smooth and plane bottom.

The results are presented as flow profiles extracted along the longitudinal axis (defined by Y = 6 m) once the fluid has reached a pseudo-equilibrium state, which occur after approximatively three minutes (Fig. 9). The flow profiles corresponding to the three different Bingham options implemented are compared with the result from the same simulation performed with MIKE21's Bingham fluid model (which is based on the same cubic equation as for Option 3) as well as with the analytical solution from [20]. The first observation that can be made is that results from all the simulations, including MIKE21, give fluid profiles characterized by a steep front and tail whereas the flow slope diminishes in the middle part of the fluid volume. Such flow profiles do not match with the theoretical parabolic shape of the analytical solution. Similar flow profiles were obtained

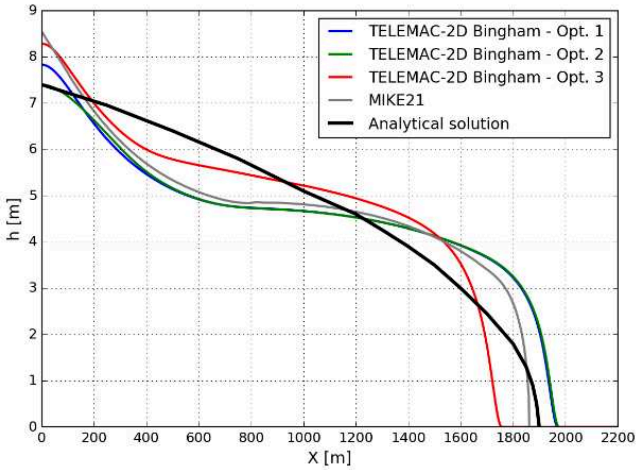

Figure 9: One-dimensional dam break, results of Bingham model compared with MIKE21 and analytical solution at pseudo-equilibrium state.

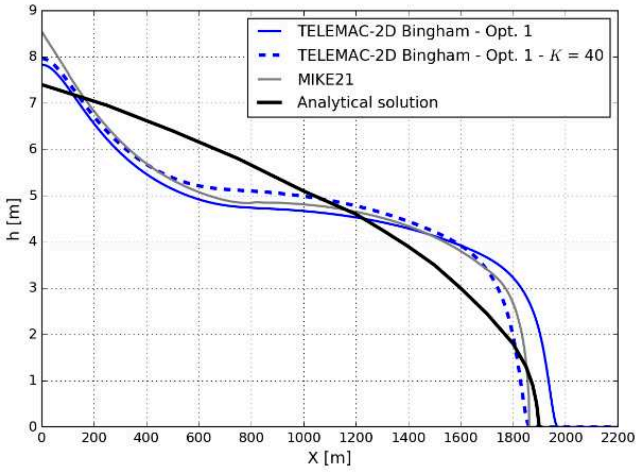

Figure 10: One-dimensional dam break, influence of the resistance parameter for laminar flow K at pseudo-equilibrium state and comparison with MIKE21 and analytical solution.

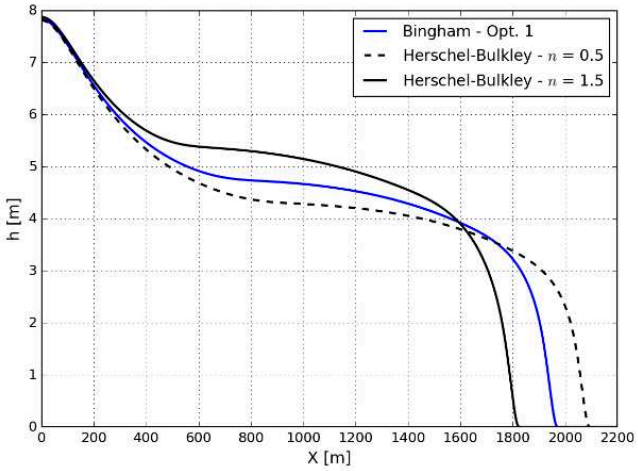

Figure 11: One-dimensional dam break, comparison between Bingham and Herschel-Bulkley models.

with the numerical code DFEM-1D for all the non-Newtonian models implemented [14]. It can be noted that in [20], it is highlighted that the assumption of a parabolic profile may not be valid in certain cases. In comparison with the flume test of thickened tailings described above, for which parabolic flow profiles were obtained, the inertial effects involved in the dam break case are not negligible which might explain the shape of the simulated flow profiles.

As for the thickened tailings case, the flow profiles obtained with the Bingham Options 1 and 2 are very close to each other, which is an expected result (see sections II-B and VI-A). The wave front is located at X = 1970 m, which corresponds to a runout distance of 1665 m that is approximatively 4.7% larger than the theoretical value. The flow profile obtained with Option 3 (Bingham cubic equation) shows a more resistive behaviour than Options 1 and 2 with a wave front located at approximatively 1750 m which corresponds to a runout distance of 1445 m that is approximatively 9.2% smaller than the theoretical value. The more resistive behaviour of the Option 3 is also an expected result (see sections II-B and VI-A) The flow profile obtained with MIKE21's Bingham model is located between the flow profiles obtained with Options 1-2 and 3, with a runout distance of approximatively 1555 m, that is 2.3% smaller than the theoretical value. The differences obtained between Option 3 and MIKE21, based on the same mathematical formulation, are likely caused by different numerical methods used in the implementation (no information regarding the numerical implementation used in MIKE21 is available [15]).

In order to test the sensibility of the Option 1 to the resistance parameter for laminar flow K, a simulation was performed with K = 40 which corresponds to an intermediate value for smooth surfaces. The result shows that the larger viscous stresses induced by this set-up steepens up the flow profile which lies very close to MIKE21's flow profile and from the theoretical solution (Fig. 10).

This dam break case has also been simulated with the Herschel-Bulkley model in which the consistency parameter K_{HB} was taken equal to the dynamic viscosity used in the Bingham simulations. Two simulations were performed with power-law index values of n = 0.5 and n = 1.5. The results are compared qualitatively with the Bingham Option 1 in Fig. 11 for the flow profiles corresponding to the pseudo-equilibrium state (after 3 minutes of simulation). As expected and in accordance with the results obtained for the thickened tailings case, a power-law index smaller than 1 (n = 0.5) shows a flatter, less resistive, profile whereas a power-law index larger than 1 (n = 1.5) shows a steeper, more resistive, profile.

In a similar way as for what is observed for the thickened tailings case, the front location spreads out in the downstream direction after that the pseudo-equilibrium state is reached due to the semi-implicit treatment used for the source term. Analysis of flow profiles obtained after 10 minutes of simulation shows that the front has migrated approximatively 70 m compared to its location after 3 minutes of simulation (when pseudo-equilibrium state is reached).

Some simulations have been run with the kinetic volume scheme (FINITE VOLUME SCHEME = 1). No significant differences were observed compared with the HLLC scheme.

The results presented above show that the non-Newtonian models implemented in TELEMAC-2D can reproduce the flow runout generated by a dam break in a satisfactory way. Inertial effects can have a significant influence on the flow profile shape. A detailed analysis of the results is recommended to identify the time at which the pseudo-equilibrium state is reached, which can be of importance for runout and flood propagation analysis.

C. Mixing between non-Newtonian and Newtonian fluids

To illustrate the pseudo-biphasic, variable-density formulation, a simple test case is used. The computational domain is composed of a mean channel reach and of a side channel discharging into the main channel with a 90-degree angle. The main channel is 90 m long and the side channel is 21 m long. Both channels are 10 m wide. The bathymetry is defined as a constant level in all the model. The computational mesh is composed of triangles with an edge side of approximatively 1 m. Two inflow boundaries are defined at the upstream end of both channels. One outflow boundary is defined at the downstream end of the main channel with a flow depth of 1 m.

Inflow of the non-Newtonian fluid is applied at the upstream end of the side channel by prescribing a discharge of 4 m^3/s and a sediment volumetric concentration C_V of 0.5 through a passive tracer. The non-Newtonian fluid density is computed by the model based on a sediment specific density ρ_S = 3000 kg/m^3 and the specified sediment volumetric concentration C_V according to (14). At the inflow boundary, the fluid's bulk density is ρ = 2000 kg/m^3. Inflow of Newtonian fluid is applied at the upstream end of the main channel by prescribing a discharge of 2 m^3/s and a nil sediment volumetric concentration through a passive tracer. The Newtonian fluid density is set to ρ_W = 1000 kg/m^3. The non-Newtonian parameters, yield stress and dynamic viscosity, are computed by the model with power laws (15) and (16) based on the local sediment volumetric concentration C_V with the following coefficients: a = 0.025, b = 8.0, c = 0.001, d = 8.0 (see section V). For the non-Newtonian fluid defined with C_V = 0.5, those coefficients yield a yield stress and dynamic viscosity of 250 Pa and 10 Pa·s, respectively while the Newtonian fluid (C_V = 0) is consequently described with a yield stress and dynamic viscosity of 0.025 Pa and 0.001 Pa·s, respectively, which is a reasonable approximation.

The model is run with the Option 1 of the Bingham model using the HLLC finite volume scheme. Bottom friction has been simulated with a Strickler coefficient of 70 m$^{1/3}$/s. Results illustrating the steady state conditions for free surface, velocity field, sediment volumetric concentration, fluid density, yield stress and dynamic viscosity are presented in Fig. 12. It can be observed that the pseudo-biphasic, variable-density formulation enables the modelling of the mixing between non-Newtonian and Newtonian fluids under the assumption that mixing is modelled through advection and diffusion of a

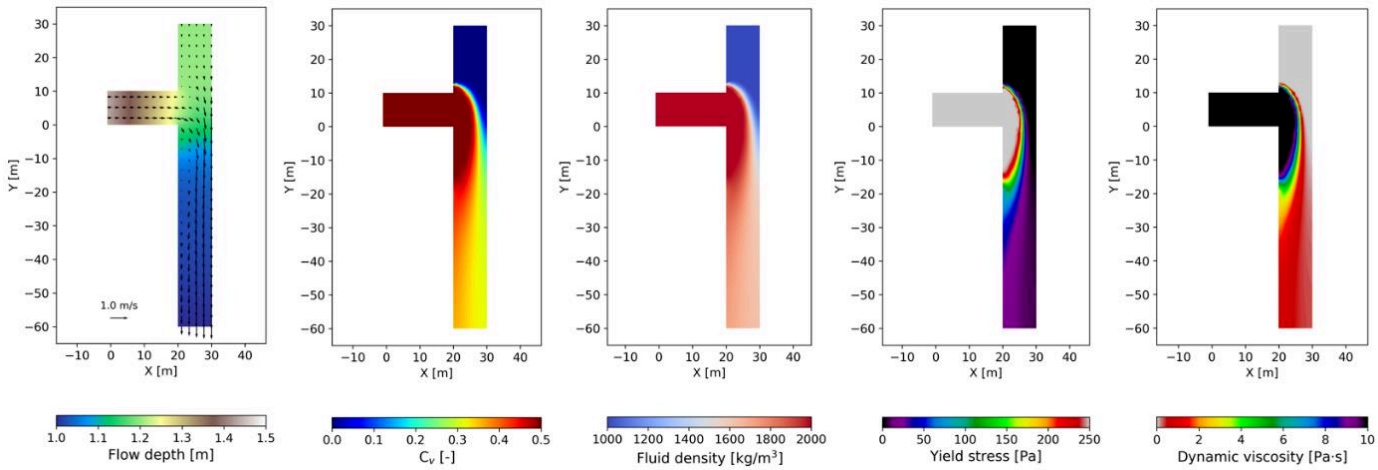

Figure 12: Mixing between non-Newtonian and Newtonian fluids, results illustrating flow conditions and rheological parameters.

passive tracer representing the sediment volumetric concentration C_V (see section V).

VII. Application example: Brumadinho tailings dam failure

On January 25, 2019, Dam I of the Córrego do Feijão mine located approximatively 9 km north-east of the city of Brumadinho (Brazil) suffered a sudden failure, caused by static liquefaction, releasing approximatively $9.7 \cdot 10^6$ m^3 of liquefied tailings within five minutes. The outflow volume represents approximatively 75% of the total storage volume of $12.7 \cdot 10^6$ m^3 (tailings and fill). The dam was approximatively 80 m high and the crest was approximatively 700 m long. The flood wave caused over 250 casualties and severe damages to the environment and infrastructure downstream of the dam site [22].

The flood wave resulting from the failure has been simulated by several teams from all over the world using different modelling tools, for example in [3], [23], [24] or [25]. Sweco has undertaken a similar work as part of an internal R&D project using the 2D hydrodynamic models MIKE21 and TELEMAC-2D. The topographical data used consists in the ALOS PALSAR RTC Digital Elevation Model (DEM) from the NASA (Alaska Satellite Facility) which describes the terrain with a 12.5 m resolution [26]. The elevation data has been acquired in 2011. Significant topographical changes occurred until the failure in the train terminal area (location A in Fig. 13) which was built after 2011 [3].

Two unstructured triangular meshes composed of 313 254 and 302 587 elements with an average edge length of 10 m was built in MIKE21. The first mesh covers the valley from upstream of the dam location down to the junction with Paraopeba River located approximately 9 km downstream of the dam while the second mesh only covers the valley from the dam toe. TELEMAC-2D simulations are based on the exact same computational meshes, converted into Selafin format with the software BlueKenue. The first mesh has been used to model the failure by letting the tailings volume be freely released at the beginning of the simulation while the second mesh was used to model the failure with an outflow hydrograph.

For the first mesh, the DEM has been processed at the dam location in order to recreate the post-failure topography so that the liquefied tailings released during the failure event could be been modelled by recreating the initial dam profile defined as initial condition for free surface in the hydrodynamic simulations. The simulated outflow volume is of approximately $10.4 \cdot 10^6$ m^3, which is 7% larger than the estimated outflow volume [22].

For the second mesh, the outflow hydrograph determined by HR Wallingford in [23] using the EMBREA-MUD tailings dam breach model has been set as a boundary condition. The hydrograph volume corresponds to the estimated released volume of $9.7 \cdot 10^6$ m^3 [22]. The peak discharge, of 90 000 m^3/s, is reached 5 s after the failure and progressively diminishes in steps until reaching 0 m^3/s after 300 s (see Fig. 13).

For the simulations in which the failure is modelled by letting the tailings volume be freely released, two hypotheses were considered: *i)* the liquefaction is supposed to be instantaneous through the overall tailings volume, *ii)* the liquefaction is supposed to be time-dependent and to propagate from the dam body towards the reservoir over time. For the first hypothesis, the simulation is performed with the nominal rheological properties of the liquefied, flowing tailings at simulation start (i.e. constant in space and time). For the second hypothesis, the tailings' rheological properties within the reservoir are defined as a function of time and location with respect to dam body, starting with very large values for yield stress and dynamic viscosity to "freeze" the fluid and progressively converging to their nominal, post-liquefaction, values. This hypothesis was modelled in TELEMAC-2D only as MIKE21 does not allow to define space and time-varying fluid properties. According to the analysis of the event detailed in [22], the failure quickly propagated from the dam body towards the reservoir while observations from surveillance cameras showed that liquefaction in the furthest parts of the reservoir occurred after approximatively 6 to 8 minutes. The instant at which

liquefaction occurs t_L [s] (i.e. when the tailings' rheological values reach their nominal values) has been modelled across the reservoir as:

$$t_L = d^{\alpha} \cdot t_{L,final} \quad (17)$$

With d a dimensionless distance [-] defined linearly between the dam body (0.0) and the outer reservoir limit (1.0), α a shape parameter [-] and $t_{L,final}$ the instant at which the furthest tailings liquefy, defined as 7 minutes (420 s). The spatial and time distribution for the liquefaction time has been modelled with a shape parameter coefficient of α = 2. This value has been chosen arbitrarily to mimic the observed release sequence [22] and the simulated outflow hydrograph [23]. It should be noted that this method is a two-dimensional simplification of the liquefaction process, that is significantly more complex [22].

Bottom friction was modelled using a Strickler coefficient of 20 $m^{1/3}/s$ in both MIKE21 and TELEMAC-2D and in both meshes and no turbulence model was used.

The available documentation regarding the rheological properties of released tailings is scarce and sometimes very different values have been used in previous works ([3] [23] [24] [25]). The bulk density of the flowing liquefied tailings used in previous studies ranges between 1800 and 3000 kg/m^3. Information from the Expert Panel Report [20] indicates that the average material's bulk density stored in the dam was about 2650 kg/m^3. Simulations have been performed with density values of ρ = 1800 and 2650 kg/m^3. A value of 1800 kg/m^3 has also been used in the MIKE21 modelling performed in [23].

According to the geotechnical data available in the Expert Panel Report [22], the tailings stored contained approximatively 50% of fine particles. The sediment volumetric concentration within the storage has been estimated to approximately C_V = 0.47. By combining this information with the available empirical relationships for yield stress (15) and dynamic viscosity (16) available in the literature ([2] [7] [18]), the yield stress and the dynamic viscosity have been assumed to lie between 100-1000 Pa and 10-100 Pa·s, respectively. Simulations have been performed with yield stress values of τ_y = 100, 500, 750 and 1000 Pa. Dynamic viscosity was set to μ = 50 Pa·s in all the simulations. Tests have shown that this parameter has limited influence on the flood wave propagation.

Available calibration data regarding water levels and flood wave propagation is scarce. The quality of the DEM is not good enough to allow for a good calibration of flow depths. According to the information available in previous studies, flood arrival time can be estimated at three locations:

- Canteen (location B in Fig. 13): ca. 2 min.
- Railway bridge (location C in Fig. 13): 10 to 12 min.
- Paraopeba River (location D in Fig. 13): 1 h 30 min to 2 h 10 min.

TELEMAC-2D simulations have been performed with the non-Newtonian Bingham model with all three implemented Options tested. Results from Options 1 and 2 are very close from each other, therefore only results from Option 1 are presented. Simulations were performed with both kinetic and HLLC finite volume schemes, no significant differences were observed. MIKE21 simulations were performed with the Bingham flow model.

Analysis of model results with respect to flood extent and flood propagation time showed that the best results were obtained with the outflow hydrograph model, a bulk density of ρ = 1800 kg/m^3, a yield stress of τ_y = 750 Pa and μ = 50 Pa·s for the dynamic density.

To illustrate the differences between the different software and modelling assumptions with respect to outflow methods, flood wave's arrival times and flood extents the following model runs are analysed:

- T-a1 = TELEMAC-2D, outflow volume freely released, Bingham Option 1.
- T-a3 = TELEMAC-2D, outflow volume freely released, Bingham Option 3.
- T-b1 = TELEMAC-2D, outflow volume freely released with time-dependent liquefaction, Bingham Option 1.
- T-b3 = TELEMAC-2D, outflow volume freely released with time-dependent liquefaction, Bingham Option 3.
- T-c1 = TELEMAC-2D, outflow hydrograph, Bingham Option 1.
- T-c3 = TELEMAC-2D, outflow hydrograph, Bingham Option 3.
- M-a = MIKE21, outflow volume freely released.
- M-c = MIKE21, outflow hydrograph.

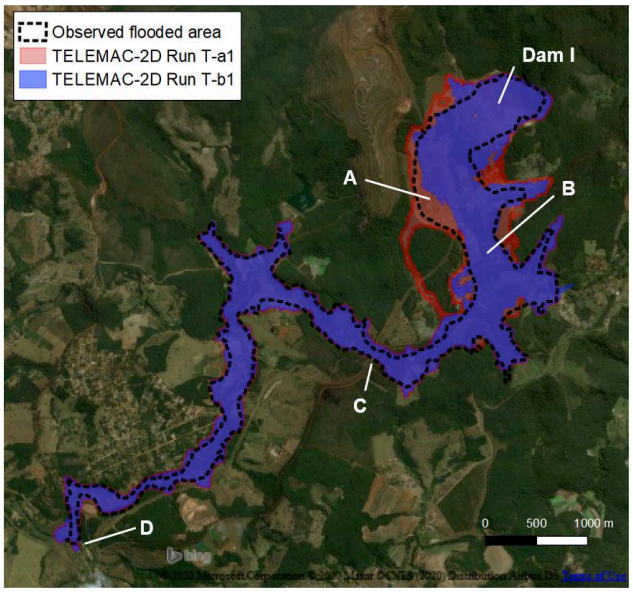

Figure 13: Brumadinho tailings dam failure, comparison of flood extents for runs T-a1 and T-b1.

TABLE 1: BRUMADINHO TAILINGS DAM FAILURE. ARRIVAL TIME AT THREE DIFFERENT LOCATIONS OBTAINED WITH THE BEST SET OF RHEOLOGICAL PARAMETERS (ρ = 1800 KG/M^3, τ_y = 750 PA, μ = 50 PA·S) AND OBSERVATIONS

Run	Canteen (B)	Railway bridge (C)	Paraopeba River (D)
T-a1	00:01:15	00:04:15	01:42:00
T-a3	00:01:15	00:04:30	01:59:00
T-b1	00:01:30	00:07:00	01:43:00
T-b3	00:01:30	00:07:15	02:00:00
T-c1	00:02:15	00:09:15	02:35:00
T-c3	00:02:15	00:09:30	02:55:00
M-a	00:01:15	00:03:45	01:51:00
M-c	00:02:00	00:07:15	02:40:00
Obs.	ca 00:02:00	ca 00:10:00-00:12:00	ca 01:30:00-02:10:00

Flood wave's arrival times are presented in Table 1 with a 15 s precision. It can be seen that the outflow release method used has a large influence flood wave propagation times, with the scenarios based on an instantaneous liquefaction ("a" runs) giving an overestimation of flood wave's celerity, especially upstream of the railway bridge (location C in Fig. 13). Scenarios based on a time-dependent liquefaction ("b" runs) or on the outflow hydrograph obtained by HR Wallingford with EMBREA-MUD [23] ("c" runs) are in better agreement with observations. Concerning the latter runs, it is worth noting that the longer propagation times obtained with TELEMAC-2D are linked to the fact that the flow regime at the inflow boundary is subcritical thus underestimating the outflow velocities and overestimating the flow depths. Comparison between MIKE21 ("M" runs) and TELEMAC-2D ("T" runs) shows that propagation times obtained with MIKE21 are slightly shorter than with TELEMAC-2D at the railway bridge but lie between TELEMAC-2D's Options 1 and 3 at the junction with Paraopeba River. The overall agreement between both software is good. Comparison between Bingham Options 1 and 3 implemented in TELEMAC-2D shows that the Option 3 give slightly slower propagation times, which is an expected result based on the more resistive behaviour of this option (see section II-B, VI-A and VI-B).

A map illustrating the maximal flood extents obtained with TELEMAC-2D with an instantaneous liquefaction (run T-a1) and with a time-dependent liquefaction (run T-b1) is presented in Fig. 13. Differences between MIKE21 and TELEMAC-2D with respect to flood extent are not significant, therefore are only results from TELEMAC-2D depicted in the map, for clarity. Results from the simulation performed with a time-dependent liquefaction are in better agreement with observations. Differences on flood extents observed between observations and model results in the railway terminal area (location A in Fig. 13) are influenced by differences between the DEM data and the actual topography when failure occurred [3]. It is worth noting that the quality of the DEM is globally poor, especially in the lower part of the flood path where high grounds are present across the valley thus creating a

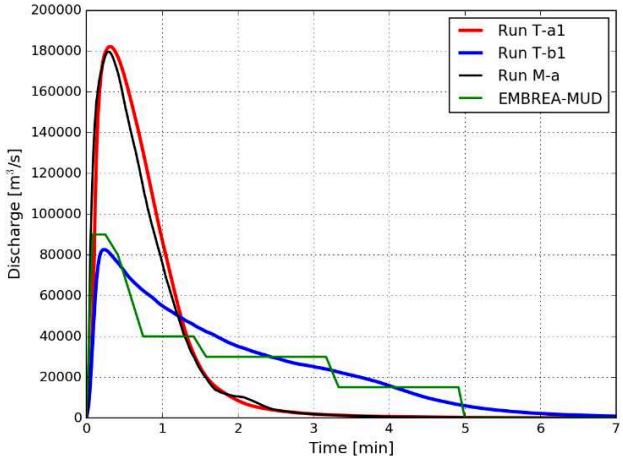

Figure 14: Brumadinho tailings dam failure, comparison of outflow hydrographs for runs T-a1 and T-b1, M-a and comparison with the hydrograph proposed by HR Wallingford using EMBREA-MUD [23].

succession of pools along the flood path which contributes to increase flow levels as well as slowing down the flood wave.

The influence of the instant at which liquefaction occurs on outflow hydrographs when modelling the release of the stored tailings is analysed by comparing the runs T-a1, M-a (instantaneous liquefaction) and T-b1 (time-dependent liquefaction), see Fig. 14. Differences between Bingham Options 1 and 3 are very small, hence only results from Option 1 are presented. The results indicate that outflows generated by an instantaneous liquefaction is characterized by a peak flow value (~180 000 m^3/s) approximatively 2.25 times greater than with a time-dependant liquefaction (~80 000 m^3/s) and consequently by a shorter outflow duration (~3 and 7 minutes, respectively). The hydrographs obtained with TELEMAC-2D (T-a1) and MIKE21 (M-a) for an instantaneous liquefaction are in good agreement. The outflow hydrograph generated with a time-dependent liquefaction (T-b1) is in good agreement with the hydrograph obtained by HR Wallingford with EMBREA-MUD [23].

Analysis of the simulations performed with ρ = 2650 kg/m^3 and for other values of yield stress τ_y between 100 and 1000 Pa, not detailed here, shows very small differences on propagation times between the dam and the railway bridge. Along this reach, the valley slope is steep (3-4% in the two first kilometres) and progressively decreases towards the railway bridge (approximatively 1%), indicating that inertial effects are likely to have a much larger influence than non-Newtonian viscous stresses on flood propagation for such configuration. On the other hand, significant differences are observed downstream of the railway bridge down to the junction with Paraopeba River where the valley slope is less pronounced (0.8-1%). For example, a density of ρ = 2650 kg/m^3 in combination with a yield stress τ_y = 750 Pa leads to approximatively 60% faster propagation time at this location compared with ρ = 1800 kg/m^3.

This case study has shown that the non-Newtonian Bingham model implemented in TELEMAC-2D in combination with a time-dependent liquefaction gives

satisfactory results for the Brumadinho tailings dam break simulation. Results compare well with similar simulations performed with MIKE21 when modelling an instantaneous liquefaction. This case study also highlights the fact that flood propagation of flowing tailings is sensitive to several key assumptions involved in such a work: dam failure mode and outflow scenario, rheological parameters (especially the fluid's density and yield stress) and quality of topographical data used. A good estimation of these parameters and their associated uncertainties is a crucial step in a tailings dam break and emergency plan study.

VIII. Conclusions and Perspectives

In this article, the non-Newtonian Bingham and Herschel-Bulkley models implemented in the Finite Volume version of TELEMAC-2D have been presented. In addition, a simplified pseudo-biphasic, variable density formulation has also been implemented in order to make it possible to model the mixing between Newtonian and non-Newtonian fluids. The validation examples presented show that these models can be used to model non-Newtonian behaviour in a satisfactory manner and compared reasonably well with results from other studies performed with other numerical codes as well as with analytical solutions. The application example of the Brumadinho tailings dam failure shows that TELEMAC-2D can be used in tailings dam break studies.

Tests have been performed in Finite Elements but showed poor performance with instabilities linked to strong source term gradients. Further work is required before the non-Newtonian models can be incorporated in TELEMAC-2D's Finite Element version. Other possible improvements would be to *i)* reduce the spreading observed in the front region once a pseudo-equilibrium state is reached, *ii)* introduce a new method for computing the shear rate by taking horizontal velocity gradients into account and *iii)* to couple the pseudo-biphasic formulation with GAIA in order to include effects of settling velocity and allow the modelling of morphological changes.

This development can be used as a base for implementing other non-Newtonian models, for example Coulomb-based models that are often used in debris-flows modelling.

This development will be included in an upcoming release of the openTELEMAC-MASCARET suite.

Acknowledgement

This work has been partly funded by Sweco as part of an internal R&D project performed together with colleague Non Okumura who was in charge of the GIS work and MIKE21 modelling involved in the Brumadinho tailings dam failure study.

The author would like to thank Riadh Ata for his support and technical guidance as well as Florent Taccone at EDF R&D for his help in incorporating this development into the openTELEMAC-MASCARET suite.

References

[1] Martin, V., Al-Mamun, M., & Small, A., CDA technical bulletin on tailings dam breach analysis, ICOLD symposium, 2019.

[2] Julien, P-Y., Erosion and sedimentation, 2nd edition, Cambridge University Press, 2010.

[3] Yu, D., Tang, L., Chen, C., Three-dimensional numerical simulation of mud flow from a tailing dam failure across complex terrain, Natural Hazards and Earth System Sciences, Vol. 20, 727-741, 2020.

[4] Gao, J., Fourie, A., Using the flume test for yield stress measurement of thickened tailings, Minerals Engineering, Vol. 81, 116-127, 2015.

[5] Blight, G. E., Bentel, G. M., The behaviour of mine tailings during hydraulic deposition, Journal of the South African Institute of Mining and Metallurgy, 1983.

[6] Chhabra, R.P., Richardson, J.F., Non-Newtonian Flow in the Process Industries. Fundamentals and Engineering Applications, Butterworth-Heinemann, 1999.

[7] FLO-2D, Simulating Mudflows, White paper available at https://flo-2d.com/downloads/ (last visit 2020-05-02).

[8] Martinez, C., Miralles-Wilhelm, F., Garcia-Martinez, R., Verification of a 2D finite element debris flow model using Bingham and cross rheological formulations, WIT Transactions on Engineering Sciences, Vol. 60, 61-69, 2008.

[9] Ajayi, A. E., Surface runoff and infiltration processes in the Volta Basin, West Africa: Observation and modeling, Ecology and Development Series, No. 18, ZEF Bonn, 2004.

[10] Mitsoulis, E., Flows of viscoplastic materials: models and computations, Rheology Reviews 2007, 135-178, 2007.

[11] Soto, H. P., et al., A Numerical Investigation of Inertia Flows of Bingham-Papanastasiou Fluids by an Extra Stress-Pressure-Velocity Galerkin Least-Squares Method, Journal of the Brazilian Society of Mechanical Sciences and Engineering, Vol. XXXII, No. 5, December-Special Issue, 2010.

[12] Shao, S., Lo, E.Y., Incompressible SPH method for simulating Newtonian and Non-Newtonian flows with a free surface, Advances in Water Resources, Vol. 26, 787-800, 2003.

[13] Rickenmann, D., Bedload transport capacity of slurry flows at steep slopes, PhD Thesis, ETH Zürich, 1990.

[14] Naef, D., et al., Comparison of flow resistance relations for debris flows using a one-dimensional finite element simulation model, Natural Hazards and Earth System Sciences, Vol. 6, 155-165, 2006.

[15] DHI, MIKE 21 Flow Model FM, Hydrodynamic Module, User Guide, 2017.

[16] EDF R&D, TELEMAC-2D, User manual, Version v8p1, 2019.

[17] Hervouet, J-M., Hydrodynamics of free surface flows, John Wiley & Sons, 2007.

[18] Oboni, F., Oboni, C., Tailings dam management for the twenty-first century. What mining companies need to know and do to thrive in our complex world, Springer International Publishing, 2020.

[19] Audusse, E., Bouchut, F., Bristeau, M. O., Klein, R., & Perthame, B. T., A fast and stable well-balanced scheme with hydrostatic reconstruction for shallow water flows, SIAM Journal on Scientific Computing, 25(6), 2050-2065, 2004.

[20] Hungr, O., A model for the runout analysis of rapid flow slides, debris flows, and avalanches, Canadian Geotechnical Journal, Vol. 32, 610-623, 1995.

[21] Toro, E. F., The HLL and HLLC Riemann solvers, In Riemann solvers and numerical methods for fluid dynamics (pp. 315-344), Springer, Berlin, Heidelberg, 2009.

[22] Robertson, P. K., et al., Report of the Expert Panel on the Technical Causes of the Failure of Feijão Dam I, 2019.

[23] Lumbroso, D., et al., Modelling the Brumadinho tailings dam failure, the subsequent loss of life and how it could have been reduced, Preprint version dated 2020-06-04, Natural Hazards and Earth System Sciences, 2020.

[24] Garcia, R., Tribst-Correa, A., Two-dimensional runout evaluation of the Brumadinho Tailings dam failure in Brazil, Conference presentation, Dam Safety, 2019.

[25] Liu, S., Back analysis of the Feijao failure, Conference presentation, Tailings and mine waste, 2019.

[26] NASA's Alaska Satellite Facility, ALOS PALSAR RTC Digital Elevation Model, https://asf.alaska.edu/data-sets/derived-data-sets/alos-palsar-rtc/alos-palsar-radiometric-terrain-correction/ (last visit 2020-05-02).